Finite-Time Fast Integral Terminal Sliding-Mode Speed Control Method With Disturbance Observer for SPMSM

Cao Li, Tianhong Pan, *Senior Member, IEEE*, and Shihong Ding, *Senior Member, IEEE*

***Abstract*—To enhance the dynamic performance and disturbance rejection of the surface-mounted permanent magnet synchronous motor (PMSM) speed control system, a new sliding-mode controller is proposed in this work. First, a new variable gain reaching law is introduced by incorporating the variable exponential and adaptive terms to reduce the time to reach the equilibrium point and suppress the chattering. Second, a new fast integral terminal sliding-mode surface is designed to improve the convergence speed, both near and away from the equilibrium point. To compensate for internal and external disturbances, an extended sliding-mode disturbance observer is developed. This new framework improves both the dynamic and steady-state performances of the system, with stability guaranteed through the Lyapunov theory. Finally, experimental results confirm that the proposed method enhances the speed response, tracking accuracy, and disturbance rejection capability in PMSM control.**

***Index Terms*—Extended sliding-mode disturbance observer (ESMDO), integral terminal sliding-mode surface, reaching law, sliding-mode controller, surface-mounted permanent magnet synchronous motor (SPMSM).**

I. Introduction

PERMANENT magnet synchronous motors (PMSMs) are widely employed in electric vehicles, robotics, aerospace, and other industrial applications due to their high power density, reliability, efficiency, and wide speed range [1], [2], [3]. In PMSM speed control, a proportional–integral (PI) controller is commonly used due to its simplicity and ease of implementation [4]. However, PMSMs are inherently nonlinear strongly coupled systems. The PI controller often struggles to cope with internal parameter variations and external disturbances, leading to suboptimal dynamic performance and disturbance rejection [5], [6].

Received 20 October 2024; revised 19 January 2025; accepted 15 March 2025. Date of publication 24 March 2025; date of current version 26 May 2025. This work was supported in part by the National Natural Science Foundation of China under Grant 62273002. Recommended for publication by Associate Editor A. M. Bazzi. *(Corresponding author: Tianhong Pan.)*

Cao Li and Tianhong Pan are with the School of Electrical Engineering and Automation, Anhui University, Hefei 230601, China (e-mail: z23101007@stu.ahu.edu.cn; thpan@ahu.edu.cn).

Shihong Ding is with the School of Electrical and Information Engineering, Jiangsu University, Zhenjiang 212013, China (e-mail: dsh@ujs.edu.cn).

Color versions of one or more figures in this article are available at https://doi.org/10.1109/TPEL.2025.3554209.

Digital Object Identifier 10.1109/TPEL.2025.3554209

To solve the speed regulation problem of the PMSM, several advanced nonlinear control methods have been proposed to enhance PMSM control performance, such as adaptive control [7], [8], model-predictive control [9], fuzzy control [10], [11], and sliding-mode control (SMC) [12], [13]. Among these existing methods, SMC has gained popularity due to its robustness to model uncertainties and fast response [4], [14].

Traditional linear SMC suffers from the inability to achieve finite-time error convergence and requires a large control gain to maintain system robustness, which inevitably intensifies chattering. In contrast, advancement in nonlinear SMC has significantly improved the dynamic performance of PMSMs [4]. The design of SMC consists of two main components: the reaching law and the sliding-mode surface [15]. The reaching law drives the system state toward the sliding-mode surface, but this process often induces chattering due to high-frequency oscillations near the surface [16]. Achieving rapid convergence to the sliding surface while maintaining an error-free system remains challenging. Various methods have been developed to mitigate chattering, including replacing the switch function with a saturation function. However, the introduction of unreasonable boundary layers in this method often results in steady-state errors [17]. In addition, several SMC-based strategies have been developed, such as modified reaching laws [18], [19], nonsingular terminal sliding modes [20], and high-order sliding mode [21]. Among these, reaching laws are particularly attractive due to their simplicity and effectiveness in improving dynamic performance [22]. In [23], the exponential sliding-mode reaching law (ESMRL) enhances system robustness and dynamic response but requires large control gains, which intensifies the level of chattering. To solve the aforementioned problems, the adaptive gain approaches have been introduced to dynamically adjust control gains and reduce chattering [24], [25]. The variable speed reaching law [5] and the terminal sliding-mode reaching law (TSMRL) [26], [27] have also been developed to improve convergence time and further suppress chattering. Meanwhile, some adaptive reaching laws are proposed to accelerate approach and obtain a limited arrival time. An adaptive exponential reaching law has been proposed to improve the reaching law while keeping a low level of chattering [28]. An inverse hyperbolic sine function combined with an exponential term has been introduced to accelerate convergence to the sliding-mode surface (SMS) [29]. By incorporating adjustable parameters, a novel adaptive

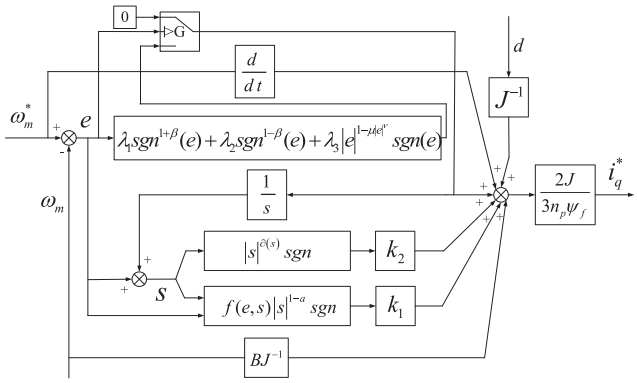

Fig. 1. Speed control block diagram of the NFITSMS with the NVGRL.

sliding mode reaching law has been designed to avoid the impact of switching functions on system performance [29].

In traditional SMC, the choice of the sliding-mode surface plays a critical role in determining system robustness and responsiveness. Nonlinear sliding-mode surfaces, such as terminal sliding-mode controller, enable finite-time convergence but often suffer from slow convergence near the equilibrium point [30]. The integral terminal sliding-mode controller (ITSMC) has been developed to improve the transient response and enable finite-time convergence [31], [32]. Adaptive integrated sliding-mode control is proposed to improve the performance of the PMSM [33]. In [34], the ITSMC is designed to realize finite-time tracking and fast transient response. In addition, to improve the robustness of the ITSMC based on the reaching law, the upper bound of the lumped disturbances is added to the control law. However, it is difficult to obtain the upper bound of unknown nonlinear lumped disturbances in practical applications [14]. At present, it is feasible to introduce disturbance observers to deal with lumped disturbances [35]. The sliding-mode observer (SMO) has been widely used in motor speed control systems because it is easy to set parameters and insensitive to load disturbances. The combination of the ITSMC with the SMO offers a promising solution by enabling real-time disturbance compensations [36], [37].

In this work, a new control strategy is proposed to enhance surface-mounted permanent magnet synchronous motor (SPMSM) speed control. This strategy enhances the system's response speed, minimizes the steady-state error during operation, and significantly improves the disturbance rejection performance. The key contributions are as follows.

1) A new variable gain reaching law (NVGRL) is proposed to balance convergence speed and chattering suppression. By incorporating system state, a variable exponential term, and an adaptive gain, the method achieves fast global tracking while effectively reducing chattering.
2) A new fast integral terminal sliding-mode surface (NFITSMS) is designed to ensure finite-time convergence, with balanced convergence rates away from and near the equilibrium point, accelerating global fast speed tracking of the SPMSM.
3) The extended sliding-mode disturbance observer (ESMDO) is developed to improve the SPMSM system's robustness against lumped disturbance, enhancing both dynamic and steady-state performances.

The rest of this article is organized as follows. Section II presents the mathematical model of the SPMSM. Section III details the design and stability analysis of the proposed NVGRL and NFITSMS controllers, along with the ESMDO. Section IV provides experimental validation of the proposed method. Finally, Section V concludes this article.

Notations: In the following sections, for $\phi > 0$, $\mathrm{sgn}^{\phi}(p)$ is represented by $|p|^{\phi}\mathrm{sgn}(p)$, $\mathrm{sgn}(\cdot)$ is the signum function, and p is any real number.

II. Problem Formulation

Under the synchronous dq rotating frame, the SPMSM mathematical model is employed as follows:

$$\dot{i}_d = \frac{1}{L}u_d - \frac{R}{L}i_d + n_p\omega_m i_q \tag{1}$$

$$\dot{i}_q = \frac{u_q}{L} - \frac{R}{L}i_q - n_p\omega_m i_d - \frac{n_p\omega_m\psi_f}{L} \tag{2}$$

$$T_e = 1.5n_p i_q\psi_f \tag{3}$$

$$J\dot{\omega}_m = T_e - B\omega_m - T_L \tag{4}$$

where u_d, u_q and i_d, i_q are the stator voltages and currents of d- and q-axes, respectively, L is the d- and q-axis stator inductance, n_p is the number of pole pairs, ω_m represents the mechanical angular speed, R is the stator resistance, ψ_f is flux linkage, T_e is the electromagnetic torque, J is the moment of inertia, B represents the damping coefficient, and $T_L$is the load torque.

Considering parameter uncertainties and external disturbance, the speed control loop equation can be expressed as

$$J\dot{\omega}_m = T_e - B\omega_m - d \tag{5}$$

where $d = T_L + \Delta B\omega_m + \Delta J\dot{\omega}_m$ is the total disturbance, and ΔJ and ΔB represent the mismatched motor parameters and external load disturbances, respectively. Defining ω_m as the control object, (5) is rewritten as

$$\dot{\omega}_m = mi_q^* - \frac{B}{J}\omega_m - \frac{d}{J} \tag{6}$$

where $m = (1.5n_p\psi_f)/J$, and i_q^* is the q-axis reference current.

As can be seen from (6), the SPMSM is sensitive to internal and external disturbances, which challenge the balance between fast response and robust disturbance rejection by using the existing SMC. The motivation is to design a new sliding-mode speed controller capable of achieving both smooth and rapid tracking under an uncertain condition and improve the dynamic and steady-state responses of the PMSM system during operation.

III. New Sliding-Mode Speed Controller

The SMC relies on two key components: the sliding-mode surface and the reaching law. The system's performance is largely determined by the appropriate design of these components.

A. Proposed NVGRL

The reaching law guides the system state toward the sliding-mode surface while maintaining the quality of the sliding phase. To balance convergence speed and chattering suppression, an NVGRL is proposed by incorporating the system state error, variable exponential term, and adaptive gain. The reaching law is given by

$$\begin{cases} \dot{s} = -k_1 f(X,s)|s|^{1-a}\text{sgn}(s) - k_2|s|^{\partial(s)}\text{sgn}(s) \\ f(X,s) = \frac{2|X|+b}{2[|X|+b\cdot\exp(-\tau|X|)]} + \frac{b\cdot\text{sgn}(|s|-1)}{2[|X|+b\cdot\exp(-\tau|X|)]} \end{cases} \tag{7}$$

where $\partial(s) = 1 + 0.5a + 0.5a\cdot\text{sgn}(|s|-1)$, $0 < a < 1$, k_1, k_2, b, and τ are positive constants, X is the system state, $\lim_{t\to 0}|X| = 0$, and s stands for the SMS function.

With the NVGRL, both low chattering and fast response are achieved. The adaptive gain term accelerates the sliding rate and suppresses chattering according to the system state. In addition, the variable exponential term is added as a pulling force to further improve the speed of reaching law. The movement trends in different stages are summarized as follows.

1) $|s| \geq 1$, i.e., the system trajectory is far away from the sliding surface. The system state arrives the sliding-mode surface according to adaptive gain term $k_1 f(X,s)|s|^{1-a}$ and exponential term $k_2|s|^{1+a}$. When the system state is far from the sliding-mode surface, $|X|$ is very large. There is $k_1 f(X,s) > k_1$; the two rates converge to $k_1 f(X,s)|s|^{1-a}$ and $k_2|s|^{1+a}$, respectively. The convergence rate to the equilibrium point is accelerated. As $|s|$ decreases, the system state moves toward the sliding surface, and chattering is also suppressed by the introduction of adaptive gain terms. At the same time, the chattering is suppressed by reducing the coefficient appropriately.
2) $|s| < 1$, i.e., the system state is close to the sliding mode surface. $k_2|s|^{1+a}$ converges to $k_2|s|$, while $k_2|s|$ is still able to converge to 0 rapidly, which avoids the overall convergence speed of the process affected by too small $k_2|s|^{1+a}$. There is $f(X,s) < 1$; the adaptive gain $k_1 f(X,s)|s|^{1-a}$ plays a dominant role. As $|s|$ decreases, obviously, the system state moves toward origin. Obviously, there is always $k_1 f(X,s) < k_1$. As $|X|$ decreases, the convergence speed is reduced. $k_1 f(X,s)$ gradually decreases and eventually converges to 0, and chattering is further suppressed.

The proposed NVGRL achieves a faster convergence than traditional methods while effectively suppressing chattering.

Theorem 1: The proposed NVGRL can ensure that s and $\dot{s}$ converge to the origin in finite time.

Proof: Set Lyapunov function $V_1(s) = 0.5s^2$, and $\dot{V}_1(s)$ is written as

$$\dot{V}_1(s) = s\left[-k_1 f(X,s)|s|^{1-a}\text{sgn}(s) - k_2|s|^{\partial(s)}\text{sgn}(s)\right]. \tag{8}$$

In (8), the value of s always has the same sign as $\text{sgn}(s)$. To satisfy the reaching condition, $\dot{V}_1(s) \leq 0$, i.e., $k_1 > 0$, $k_2 > 0$, $b > 0$, $\tau > 0$, and $0 < a < 1$. Therefore, $\dot{V}_1(s)$ is always less than or equal to 0, and the NVGRL satisfies the sliding-mode reaching condition.

Assume that the initial state of the system is $s_0 \geq X_0 > 1$. The reaching process can be divided into two distinct stages: $s_0 \to s = 1$ and $s = 1 \to 0$. Referring to the proof process in [38], the reaching time T_1 can be rewritten as follows:

$$\begin{aligned} T_1 = & \int_0^1 \frac{ds}{k_1 f(X,s)s^{1-a} + k_2 s} + \int_1^{|s_0|} \frac{ds}{k_1 f(X,s)s^{1-a} + k_2|s|^{1+a}} \\ < & \frac{1}{a}\int_0^1 \frac{d(s^a)}{k_1 f(X_0,s) + k_2 s^a} + \frac{1}{a}\int_1^{|s_0|} \frac{d(s^a)}{k_1 + k_2 s^{2a}} \\ < & \frac{1}{ak_2}\ln\left|1 + \frac{k_2}{k_1}(1+b)\right| + \frac{1}{a\sqrt{k_2 k_1}}\arctan\left(\frac{\sqrt{k_2}|s_0|^a}{\sqrt{k_1}}\right) \\ < & \frac{1}{ak_2}\ln\left|1 + \frac{k_2}{k_1}(1+b)\right| + \frac{\pi}{2a\sqrt{k_2 k_1}}. \end{aligned} \tag{9}$$

Remark 1: From (9), the reaching time T_1 is less than a value independent of the initial state s_0. By setting reasonable parameters, the system state will converge to the origin in finite time.

In practical applications, the real-time controller operates within a sliding-mode bandwidth. To further analyze the chattering phenomenon in the NVGRL, the bandwidth is computed from a discrete perspective when the system state is close to the sliding-mode surface. At this point, the NVGRL is simplified to

$$\dot{s} = -\frac{k_1|X|}{|X| + b\cdot\exp(-\tau|X|)}|s|^{1-a}\text{sgn}(s). \tag{10}$$

The discrete form of (10) can be obtained

$$\begin{aligned} s_{n+1} - s_n &= -\frac{k_1|X_n|}{|X_n| + b\cdot\exp(-\tau|X_n|)}T|s_n|^{1-a}\text{sgn}(s_n) \\ &\leq -\frac{k_1|X|}{|X_n| + b\cdot\exp(-\tau|X_n|)}T|X_n|^{1-a}\text{sgn}(s_n) \end{aligned} \tag{11}$$

where T is the sampling time.

The system trajectory is assumed to reach the sliding-mode surface within finite step, which results in $s_n = 0^+$ or $s_n = 0^-$. The next periodic equation can be updated as

$$\begin{cases} s_{n+1} \leq -\frac{k_1|X_n|}{|X_n| + b\cdot\exp(-\tau|X_n|)}T|X_n|^{1-a}, s(n) = 0^+ \\ s_{n+1} \leq \frac{k_1|X_n|}{|X_n| + b\cdot\exp(-\tau|X_n|)}T|X_n|^{1-a}, s(n) = 0^-. \end{cases} \tag{12}$$

According to (12), the discrete chattering boundary Δ for (11) is

$$\Delta \leq \frac{2k_1|X_n|}{|X_n| + b\cdot\exp(-\tau|X_n|)}T|X_n|^{1-a}. \tag{13}$$

Remark 2: As X decreases, the NVGRL reduces the chattering within the boundary of the system trajectory, which prevents the system state from converging to the equilibrium point.

B. New Fast Integral Terminal Sliding-Mode Surface

In SMC, the sliding-mode surface determines the system's trajectory. By combining the integral-type and terminal-type

sliding mode, the need for speed derivative information is eliminated. In addition, introducing a nonlinear term into the SMC accelerates the convergence rate of the speed error and ensures finite-time convergence of the system.

According to (6), the speed tracking error is defined as e. Thus, the NFITSMS is designed as

$$s = e + \int_0^t \left(\lambda_1 \mathrm{sgn}^{1+\beta}(e) + \lambda_2 \mathrm{sgn}^{1-\beta}(e) + \lambda_3 |e|^{1-\mu|e|^{\nu}} \mathrm{sgn}(e)\right) dt \tag{14}$$

where $e = \omega_m^* - \omega_m$, ω_m^* is reference mechanical angular speed, λ_1, λ_2, and λ_3 are positive constants, and $0 < \beta < 1$, $\mu > 0$, and $v > 0$.

When the tracking error reaches the sliding surface, there exists $\dot{s} = 0$. The derivative of (14) is described as

$$\dot{e} = -\lambda_1 \mathrm{sgn}^{1+\beta}(e) - \lambda_2 \mathrm{sgn}^{1-\beta}(e) - \lambda_3 |e|^{1-\mu|e|^{\nu}} \mathrm{sgn}(e). \tag{15}$$

Assumption 1: For the system described by (6), d and its derivatives are differentiable and bounded.

Remark 3: In actual operation, the SPMSM parameters, reference speed, and current are bounded, and reaction time is required for loading and unloading. Thus, Assumption 1 is reasonable.

Lemma 1 [39]: Consider a nonlinear system

$$\dot{e} = f(e), e(0) = e_0 \tag{16}$$

where $e \in \mathcal{R}^n$, and $f(e)$ is a continuous function. There exists a Lyapunov function $V(e)$, expressed as

$$\dot{V}(e) + uV^{\rho}(e) \le 0. \tag{17}$$

For any given initial condition $e(0) = e_0$, the sliding-mode equilibrium point $e = 0$ is globally finite-time stable, with the settling time T_r given by

$$T_r \le \frac{V(e_0)^{1-\rho}}{u(1-\rho)} \tag{18}$$

where $u > 0$ and $0 < \rho < 1$.

Theorem 2: The new sliding-mode dynamic (15) is finite-time stable, and the tracking error converges to the equilibrium point in this time.

Proof: Define the Lyapunov function

$$V_2(e) = 0.5e^2. \tag{19}$$

The derivative of $V_2(e)$ is as follows:

$$\begin{aligned} \dot{V}_2(e) &= -\lambda_1 |e|^{2+\beta} - \lambda_2 |e|^{2-\beta} - \lambda_3 |e|^{2-\mu|e|^{\nu}} \\ &\le -\lambda_1 |e|^{2+\beta} - \lambda_2 |e|^{2-\beta} \\ &\le -\lambda_2 2^{\frac{2-\beta}{2}} V_2^{\frac{2-\beta}{2}}(e). \end{aligned} \tag{20}$$

According to Lemma 1, the convergence time is bounded by

$$T_r \le \frac{V(e_0)^{1-\rho}}{u(1-\rho)} = \frac{V_2(e_0)^{[1-(2-\beta)/2]}}{\lambda_2 \cdot 2^{2-\beta}\,[1-(2-\beta)/2]}. \tag{21}$$

To prove the issue clearly, the settling time is determined by

$$\begin{aligned} T_2 &= \int_0^{|e_0|} \frac{de}{\lambda_1 e^{1+\beta} + \lambda_2 e^{1-\beta} + \lambda_3 e^{1-\mu|e|^{\nu}}} \\ &< \int_0^1 \frac{de}{\lambda_1 e^{1+\beta} + \lambda_2 e^{1-\beta}} + \int_1^{|e_0|} \frac{de}{\lambda_1 e^{1+\beta} + \lambda_2 e^{1-\beta}} \\ &= \int_0^1 \frac{de}{e^{1-\beta}\left(\lambda_1 e^{2\beta} + \lambda_2\right)} + \int_1^{|e_0|} \frac{de}{e^{1-\beta}\left(\lambda_1 e^{2\beta} + \lambda_2\right)} \\ &= \frac{\arctan(\sqrt{\lambda_1/\lambda_2} e_0^{\beta})}{\beta\sqrt{\lambda_1\lambda_2}} < \frac{\pi}{2\beta\sqrt{\lambda_1\lambda_2}}. \end{aligned} \tag{22}$$

The tracking error can quickly converge to the equilibrium point by appropriately setting λ_1, λ_2, and β.

Remark 4: For (14), the tracking error can converge to the origin within a maximum settlement time, which is independent of the initial state e_0. When the system state is far from the equilibrium state, $\lambda_1 \mathrm{sgn}^{1+\beta}(e)$ dominates to ensure a fast convergence rate. When the system state approaches equilibrium, the system converges quickly under the action of $\lambda_2 \mathrm{sgn}^{1-\beta}(e)$. Meanwhile, $\lambda_3 |e|^{1-\mu|e|^{\nu}} \mathrm{sgn}(e)$ has little effect when the system state is far from equilibrium, avoiding aggravated integral saturation. Furthermore, it can adjust the speed of the system state as it approaches equilibrium, and the system can be guaranteed to finite-time convergence. Fast global convergence of the tracking error is achieved.

C. Design of the Speed Controller Based on the NVGRL and the NFITSMS

The sliding-mode speed controller is designed to maintain the actual motor speed closely aligned with the reference speed. Let $e = X$; substituting (7) into (14) yields

$$\begin{aligned} &\dot{e} + \lambda_1 \mathrm{sgn}^{1+\beta}(e) + \lambda_2 \mathrm{sgn}^{1-\beta}(e) + \lambda_3 |e|^{1-\mu|e|^{\nu}} \mathrm{sgn}(e) \\ &= -k_1 f(e,s) |s|^{1-a} \mathrm{sgn}(s) - k_2 |s|^{\partial(s)} \mathrm{sgn}(s). \end{aligned} \tag{23}$$

Then, combining this with the dynamic equation (6), the corresponding block diagram of the control law is shown in Fig. 1, and the control law can be designed as

$$\begin{aligned} i_q^* = \frac{1}{m} \Bigg[&\dot{\omega}_m^* + \frac{B}{J}\omega_m + \frac{d}{J} \\ &+ \lambda_1 \mathrm{sgn}^{1+\beta}(e) + \lambda_2 \mathrm{sgn}^{1-\beta}(e) + \lambda_3 |e|^{1-\mu|e|^{\nu}} \mathrm{sgn}(e) \\ &+ k_1 f(e,s) |s|^{1-a} \mathrm{sgn}(s) + k_2 |s|^{\partial(s)} \mathrm{sgn}(s) \Bigg]. \end{aligned} \tag{24}$$

Remark 5: When the motor starts or undergoes sudden speed changes, the integral term in the controller can lead to speed overshoot, which negatively impacts speed control accuracy. To solve this problem, an integral separation approach is adopted. A threshold is set according to the speed error, and then, the action time of the integral term is controlled. This method helps reduce overshoot and improves overall control performance.

D. Design of the ESMDO

As shown in (24), the internal and external disturbances significantly impact the controller performance. To enhance the controller's robustness against such disturbances, an ESMDO is designed to estimate the disturbance in real time and provide compensation to i_q^* through feedback. Considering the disturbance d as the state variable, the state-space equation of system is denoted by

$$\begin{bmatrix}\dot{\omega}_m\\ \dot{d}\end{bmatrix}=\begin{bmatrix}-\frac{B}{J} & -\frac{1}{J}\\ 0 & 0\end{bmatrix}\begin{bmatrix}\omega_m\\ d\end{bmatrix}+\begin{bmatrix}\frac{1}{J}\\ 0\end{bmatrix}T_e. \tag{25}$$

The mechanical angular speed and disturbance are considered as observed variables; the extended state equation is expressed as follows:

$$\begin{bmatrix}\dot{\hat{\omega}}_m\\ \dot{\hat{d}}\end{bmatrix}=\begin{bmatrix}-\frac{B}{J} & -\frac{1}{J}\\ 0 & 0\end{bmatrix}\begin{bmatrix}\hat{\omega}_m\\ \hat{d}\end{bmatrix}+\begin{bmatrix}\frac{1}{J}\\ 0\end{bmatrix}T_e+\begin{bmatrix}1\\ l\end{bmatrix}g(e_m) \tag{26}$$

where $\hat{\omega}_m$ and $\hat{d}$ are the estimated values of the mechanical angular speed and disturbance, respectively, $g(e_m)$ is the observer control function corresponding to the mechanical angular velocity observation error $e_m=\omega_m-\hat{\omega}_m$, and l is the observer gain. Combining (25) and (26), the observation error is described as

$$\begin{cases}\dot{e}_m=-\frac{B}{J}e_m-\frac{1}{J}e_d-g(e_m)\\ \dot{e}_d=-l\cdot g(e_m)\end{cases} \tag{27}$$

where $e_d=d-\hat{d}$ is the disturbance observation error. The sliding-mode surface is chosen as

$$s_m=e_m+c_m\int_0^t e_m dt \tag{28}$$

where c_m is a positive constant. The reaching law is set as

$$\dot{s}_m=-k_3\mathrm{sgn}(s_m) \tag{29}$$

where k_3 is the positive constant.

To ensure that the observation error e_m converges to zero in finite time, $g(e_m)$ is written as

$$g(e_m)=\left(c_m-\frac{B}{J}\right)e_m+k_3\mathrm{sgn}(s_m). \tag{30}$$

In order to satisfy the condition that the observer trajectory can reach and stay on the sliding-mode surface in finite time, the following conditions should also be satisfied:

$$\begin{cases}s_m=\dot{s}_m=0\\ \dot{e}_m=e_m=0.\end{cases} \tag{31}$$

Combining (27) and (31) yields

$$\begin{cases}e_d=-J\cdot g(e_m)\\ \dot{e}_d=-l\cdot g(e_m).\end{cases} \tag{32}$$

The integration of (32) yields

$$e_d=\kappa\cdot\exp(lt/J) \tag{33}$$

where κ is a constant. When l satisfies $l<0$, the observer error converges to 0.

Therefore, the tracking error can converge to 0 in finite time by choosing appropriate observer gains. The final ESMDO structure is shown in Fig. 2.

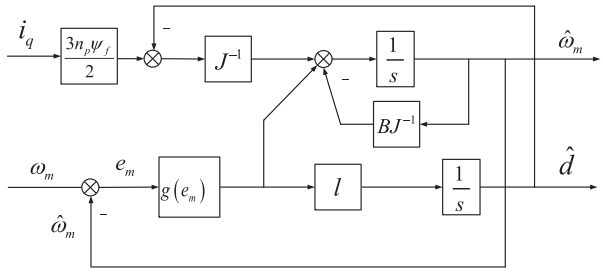

Fig. 2. Block diagram of the ESMDO.

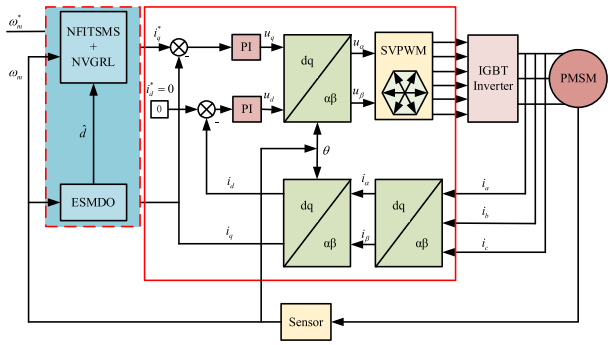

Fig. 3. Proposed control structure of the SPMSM speed drive system.

E. Stability Proof of the Proposed Sliding-Mode Speed Controller

The proposed new sliding-mode speed controller structure (NFITSMS + NVGRL + ESMDO) of the SPMSM system based on the field-oriented control approach is shown in Fig. 3.

The estimated disturbance is compensated by feedback to the controller; (24) can be rewritten as

$$\begin{aligned}i_q^*=\frac{1}{m}\Bigg[&\dot{\omega}_m^*+\frac{B}{J}\omega_m+\frac{\hat{d}}{J}\\ &+\lambda_1\mathrm{sgn}^{1+\beta}(e)+\lambda_2\mathrm{sgn}^{1-\beta}(e)+\lambda_3|e|^{1-\mu|e|^\nu}\mathrm{sgn}(e)\\ &+k_1f(e,s)|s|^{1-a}\mathrm{sgn}(s)+k_2|s|^{\partial(s)}\mathrm{sgn}(s)\Bigg].\end{aligned} \tag{34}$$

Using the Lyapunov function $V_3(s)=0.5s^2$, the derivative of $V_3(s)$ is rewritten as

$$\begin{aligned}\dot{V}_3(s)&=s\left[\dot{e}+\lambda_1\mathrm{sgn}^{1+\beta}(e)+\lambda_2\mathrm{sgn}^{1-\beta}(e)+\lambda_3|e|^{1-\mu|e|^\nu}\mathrm{sgn}(e)\right]\\ &=s\Bigg[\dot{\omega}_m^*-\frac{3n_p\psi_f}{2J}i_q+\frac{B}{J}\omega_m+\frac{\hat{d}}{J}\\ &\quad+\lambda_1\mathrm{sgn}^{1+\beta}(e)+\lambda_2\mathrm{sgn}^{1-\beta}(e)+\lambda_3|e|^{1-\mu|e|^\nu}\mathrm{sgn}(e)\Bigg]\\ &=-s\left[k_1f(e,s)|s|^{1-a}\mathrm{sgn}(s)+k_2|s|^{\partial(s)}\mathrm{sgn}(s)\right]\le 0.\end{aligned} \tag{35}$$

Therefore, the designed sliding-mode speed controller is asymptotically stable, and the tracking error can converge to 0 in finite time.

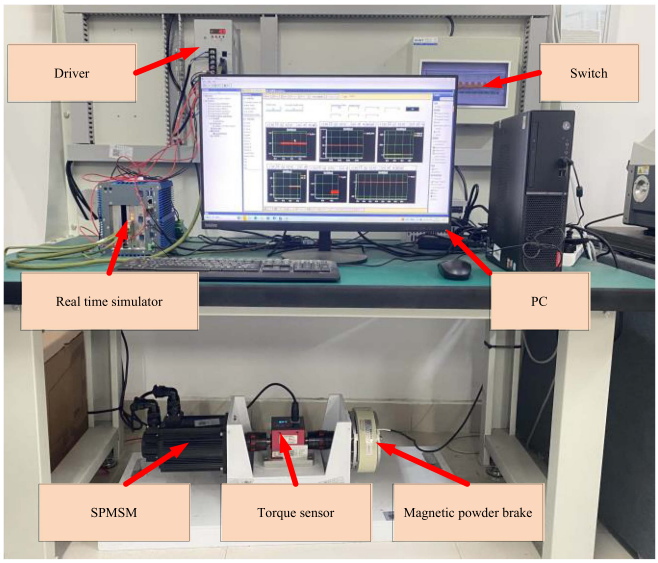

Fig. 4. Experimental platform.

F. Parameter Tuning Guidelines

In practical engineering applications, a clear method for tuning controller parameters is essential. To simplify the tuning process, the steps are outlined as follows.

1) *Initial parameter setup:* Begin by setting initial values for $\lambda_3 = 0$, $0 < a = \beta < 1$, using (8) and (21), determine a set of data that allows the motor to operate.
2) *Adjusting key parameter:* Keep other parameters unchanged, and gradually increase λ_1, λ_2, k_1, k_2, and G. If overshooting occurs, reduce these values accordingly.
3) *Fine-tuning for performance:* Adjust τ and b according to practical requirements for signal smoothing and convergence speed. To achieve desired robustness and the fast convergence while reducing chattering, increase λ_3 and μ or decrease ν as needed.
4) *Final optimization:* Fine-tune parameters by considering chattering levels and control input amplitude to achieve optimal performance.

Remark 6: During the tuning process, the order of parameter adjustment is crucial. Parameters with minimal impact can be simplified or temporarily ignored, while those with similar effects are tuned together in the same step. This approach ensures simple and clear control results.

IV. Experiments

To validate the effectiveness of the proposed method, a series of experiments was conducted. The control performance of the proposed method was evaluated through comparative analysis with other existing methods. The experimental platform, built to verify the system's performance, consists of an SPMSM, a driver, a real-time simulator, a PC, a magnetic powder brake, and a torque sensor, as shown in Fig. 4. The parameters of the PMSM are listed in Table I, the controller parameters of the involved methods are shown in Table II.

TABLE I
Parameters of the SPMSM

Symbol	Name	Value
n	Rated speed	1000 rpm
R	Stator resistance	0.8950 Ω
L	Stator inductance	3.1 mH
ψ_f	Rotor flux linkage	0.2534 Wb
J	Moment of inertia	0.0018 kg m^2
B	Damping coefficient	8.969×10^{-5} N·m·s
n_p	Number of poles	4

TABLE II
Parameters of the Controller

Name	Values
PI	$k_{pc} = 8$, $k_{ic} = 500$ (Current loop) $k_{ps} = 0.15$, $k_{is} = 0.65$ (Speed loop)
ESMRL	$k_1 = 10$, $k_2 = 4$
TSMRL	$k_1 = 10$, $k_2 = 4$, $a = 0.5$
NVGRL	$k_1 = 10$, $k_2 = 4$, $a = 0.5$, $b = 10$, $\tau = 0.5$
NFITSMS	$\beta = 0.4$, $\lambda_1 = 5$, $\lambda_2 = 10$, $\lambda_3 = 15$, $\mu = 5$, $\nu = 0.5$, $G = 20$
FITSMS	$\beta_1 = 0.6$, $\lambda_1 = 5$, $\lambda_2 = 10$
ESMDO	$c_m = 10$, $k_3 = 500$, $l = -2$

To assess the performance of the proposed NFITSMS + NVGRL + ESMDO, a comparative analysis was performed against the following methods: PI control, NFITSMS + ESMRL, NFITSMS + TSMRL, and NFITSMS + NVGRL. Furthermore, to verify the effectiveness of proposed NFITSMS, the comparison experiments were carried out against the fast integral terminal sliding-mode surface (FITSMS). The experiments were designed to measure the speed and q-axis current of the PMSM under various conditions, including start-up, load addition, parameter mismatches, and random noise. The composite controller was applied to the speed control system of the PMSM to evaluate its dynamic and steady-state performance under these scenarios.

A. Start-Up and Steady-State Performance Under No Load

As shown in Fig. 5, after reaching the reference speed, the speed fluctuations for four methods are 3.9, 4.5, 3.6, and 3.6 r/min. The NFITSMS with the NVGRL achieved a start-up time of 0.334 s, which is significantly faster than the other methods, with start-up times of 1.221, 0.413, and 0.386 s. When the speed error is large, the variable exponential term $k_2|s|^{1+a}$ accelerates the system's convergence to the sliding-mode surface. Once the sliding-mode surface is reached, the adaptive term $k_1 f(X, s)|s|^{1-a}$ gradually reduces the driving speed error to 0, thereby minimizing the system chattering.

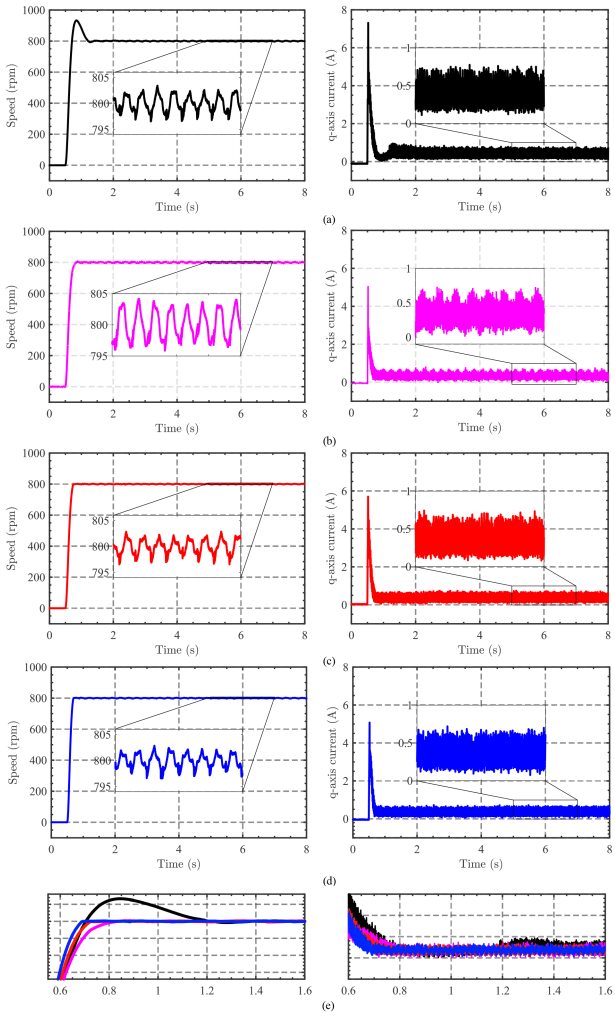

Fig. 5. Experimental results at the startup time. (a) PI control. (b) ESMRL. (c) TSMRL. (d) NVGRL. (e) Local variations of speed and q-axis current.

TABLE III
PERFORMANCE INDEXES OF FOUR METHODS

Symbol	Setting time (s)	Speed IAE	Speed RMSE
PI	1.221	0.6436	1.5177
NFITSMS + ESMRL [23]	0.413	1.3554	2.2026
NFITSMS + TSMRL [26]	0.386	0.5064	1.3461
NFITSMS + NVGRL	0.334	0.4845	1.3168

Meanwhile, to further evaluate the performance of the proposed method, the integral absolute error (IAE), denoted as $\text{IAE} = \sqrt{1/N}\sum_{i=1}^{N}(\omega_m(i) - \omega_{\text{avg}})^2/\omega_{\text{avg}}$, and the root-mean-square error (RMSE), denoted as $\text{RMSE} = (\sum_{i=1}^{N}|e(i)|^2/N)^{1/2}$, were calculated to assess the speed response in steady-state processes. At $3 < t < 8$, the specific comparative results of these four control methods are presented in Table III. The results indicate that the proposed NVGRL provides the SPMSM with lower speed error and faster dynamic response compared to other methods.

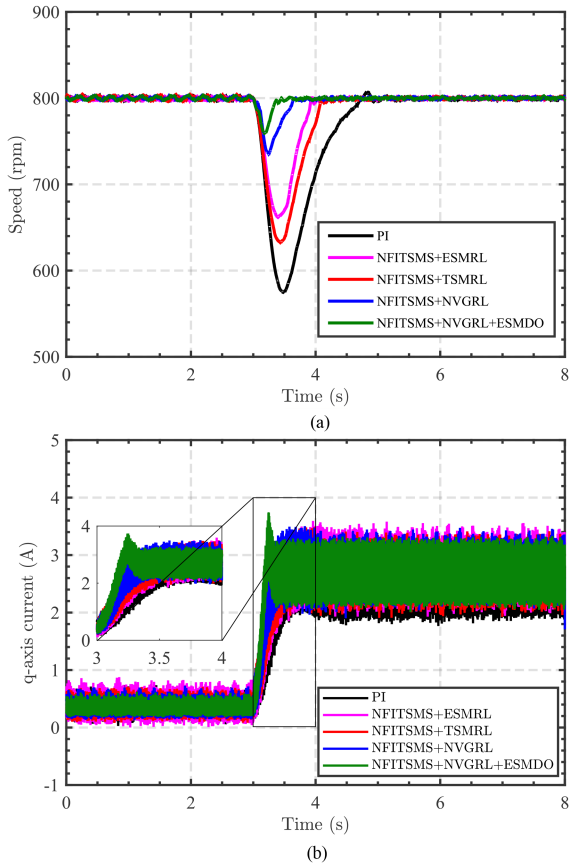

Fig. 6. Experimental results with the load of 4.6 N·m. (a) Speed responses. (b) q-axis current responses.

B. Speed Response Under Sudden Load Changes

In this experiment, the reference speed was set to 800 r/min, and both speed and q-axis current response were recorded under a load of 4.6 N·m. As shown in Fig. 6, compared with the PI control method, the proposed NFITSMS results in a steeper rise phase, which accelerates the convergence of the speed error. The NVGRL improves both the convergence speed and system robustness, utilizing variable exponential terms, in contrast to other reaching laws. As the system approaches the reference speed, the variable exponential term converges to 0 faster than the adaptive term. The adaptive term gradually decreases to 0, slowing down the speed convergence and reducing chattering. Furthermore, the addition of the ESMDO enhances the disturbance resistance and reduces the stabilization time. The settling times for the speed response were 1.751, 1.624, 1.483, 1.082, and 0.631 s for the different control methods. The corresponding speed drops for each method were 224, 167, 136, 65, and 41 r/min. From the q-axis current perspective, NVGRL and NVGRL + ESMDO methods demonstrated smaller ripples and reduced chattering compared with other methods. At $6 < t < 8$, the IAE and the RMSE are calculated to evaluate the magnitude of the five methods. Detailed disturbance rejection performance indexes for all five control schemes are shown in Table IV. The results show that the proposed method has less speed fluctuation, and bold values are used to highlight the effectiveness of the proposed method.

TABLE IV
PERFORMANCE INDEXES OF FIVE METHODS

Symbol	Setting time (s)	Speed drop (r/min)	Speed IAE	Speed RMSE
PI	1.751	224	0.2565	1.2045
NFITSMS + ESMRL[23]	1.624	167	0.1380	0.8835
NFITSMS + TSMRL[26]	1.483	136	0.1327	0.8665
NFITSMS + NVGRL	1.082	65	0.1187	0.8293
NFITSMS+NVGRL+ESMDO	**0.631**	**41**	**0.1143**	**0.8043**

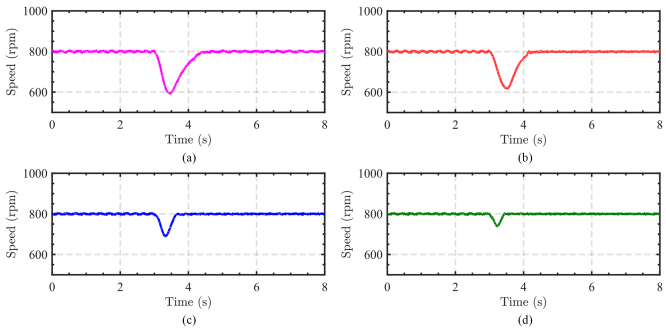

Fig. 7. Speed responses of four methods at 0.5J mismatch with the load of 4.6 N·m based on NFITSMS. (a) ESMRL. (b) TSMRL. (c) NVGRL. (d) NVGRL + ESMDO.

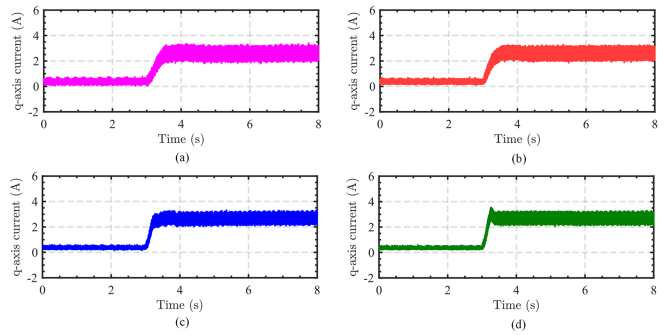

Fig. 8. q-axis current responses of four methods at 0.5 J mismatch with the load of 4.6 N·m based on NFITSMS. (a) ESMRL. (b) TSMRL. (c) NVGRL. (d) NVGRL + ESMDO.

C. Speed Response Under Parameters Change

The parameters of the SPMSM may vary during actual operation, and the reference parameters may differ from the actual values. According to the control law, the speed control effect will be affected by the change of J [40]. To verify the robustness of the proposed method, the speed and q-axis current responses were analyzed under a rotational inertia mismatch condition. The mismatch of 0.5 J was introduced, as shown in Figs. 7 and 8. According to the control law, the speed loop will be affected when the parameters are mismatched. The traditional approach law is greatly affected by this disturbance, and the response speed is slow. Due to the larger variable exponential term, the proposed convergence law mitigates the effect under this perturbation.

TABLE V
PERFORMANCE INDEXES OF FOUR METHODS AT 0.5 J

Symbol	Setting time (s)	Speed drop (r/min)	Speed IAE	Speed RMSE
NFITSMS + ESMRL [23]	1.748	206	0.1380	0.8635
NFITSMS + TSMRL [26]	1.685	180	0.1273	0.8471
NFITSMS + NVGRL	1.190	109	0.1187	0.8193
NFITSMS + NVGRL+ ESMDO	**0.716**	**59**	**0.1081**	**0.7849**

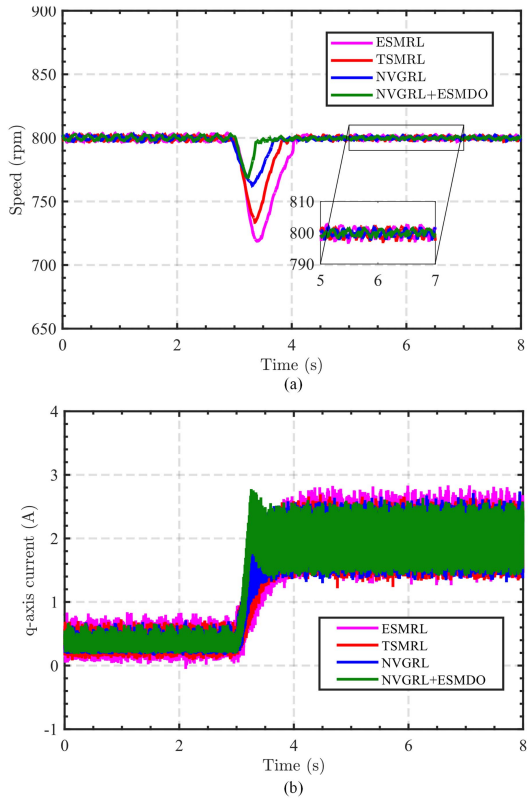

Fig. 9. Speed responses and q-axis current responses of four methods at 2 J mismatch with the load of 2.6 N·m based on the NFITSMS. (a) Speed responses. (b) q-axis current responses.

In Fig. 7, the settling times for the speed response were 1.748, 1.685, 1.190, 1.082, and 0.716 s for the different control methods. The speed drops for the different methods were 206, 180, 109, and 59 r/min, demonstrating that the proposed method exhibits superior antidisturbance performance. As shown in Fig. 8, the proposed method produces lower current ripple. At $6 < t < 8$, the IAE and the RMSE are calculated to evaluate the magnitude of the four methods. The results show that the proposed method reduced speed magnitude compared with the ESMRL, the TSMRL, and the NVGRL under 0.5 J mismatch condition. The evaluated results are illustrated in Table V, further highlighting the superior performance of the proposed method.

As shown in Fig. 9, the mismatch of 2 J was introduced at 800 r/min with 2.6 N·m load. In the steady state, the adaptive term ensures that the system has a low chattering. The speed

TABLE VI
PERFORMANCE INDEXES OF FOUR METHODS AT 2 J

Symbol	Setting time (s)	Speed drop (r/min)	Speed IAE	Speed RMSE
NFITSMS + ESMRL [23]	1.595	81	0.2429	1.3309
NFITSMS + TSMRL [26]	1.364	62	0.1647	1.1803
NFITSMS + NVGRL	1.118	38	0.1421	0.9677
NFITSMS + NVGRL + ESMDO	**0.619**	**22**	**0.1093**	**0.8089**

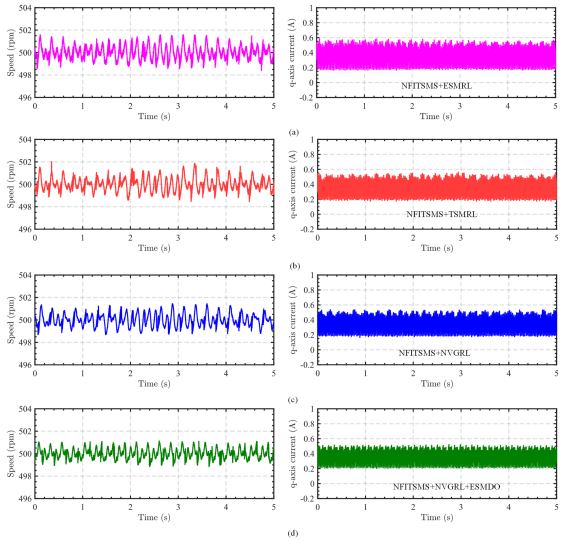

Fig. 10. Speed response and the q-axis current response of four methods at 0.5 J mismatch with 500 r/min. (a) ESMRL. (b) TSMRL. (c) NVGRL. (d) NVGRL + ESMDO.

drops for the different methods were 82, 66, 39, and 30 r/min. The proposed method produces lower current ripple compared with the ESMRL, the TSMRL, and the NVGRL. The evaluated results are illustrated in Table VI. It can be seen that the proposed controller is more insensitive to the mismatch condition.

Furthermore, to further verify the performance of speed regulation under parameter mismatch, the changes of speed and q-axis current were measured under a 0.5 J mismatch condition at 500 r/min. In the steady state, the sliding-mode chattering is reduced under the action of the adaptive term, and the internal disturbance was observed by the ESMDO. As shown in Fig. 10, the parameter mismatch causes instability in the speed waveforms for most methods. However, the proposed method effectively suppresses these unsteady waveforms, achieving smoother speed and q-axis current responses. The specific comparative results of these four control schemes are presented in Table VII. Under this condition, both the speed and the current show that the chattering was reduced with the proposed reaching law. The proposed SMC method effectively observes the parameter mismatch disturbance, leading to weakened speed fluctuations.

TABLE VII
PERFORMANCE PARAMETERS OF FOUR METHODS AT 500 R/MIN

Symbol	Speed IAE	Speed RMSE
NFITSMS + ESMRL [23]	0.1682	0.6140
NFITSMS + TSMRL [26]	0.1563	0.5912
NFITSMS + NVGRL	0.1473	0.5741
NFITSMS + NVGRL + ESMDO	**0.0914**	**0.4520**

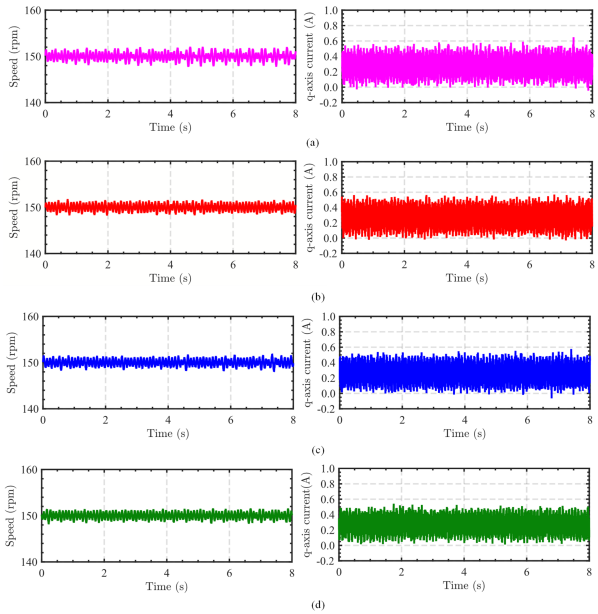

Fig. 11. Speed response and the q-axis current response of four methods with random noise at 150 r/min. (a) ESMRL. (b) TSMRL. (c) NVGRL. (d) NVGRL + ESMDO.

TABLE VIII
TRANSIENT PERFORMANCE INDEXES OF FOUR METHODS WITH RANDOM NOISE

Symbol	Speed IAE	Speed RMSE
NFITSMS + ESMRL [23]	1.2654	0.8301
NFITSMS + TSMRL [26]	0.9428	0.7078
NFITSMS + NVGRL	0.8548	0.6712
NFITSMS + NVGRL + ESMDO	**0.8354**	**0.6651**

D. Steady-State Response at Low Speed With Random Noise

The SPMSM is particularly susceptible to sensor noise at low speed. To evaluate the immunity performance of the proposed method under such conditions, random noise with an amplitude of 0.1 was introduced at 150 r/min, and the steady-state performance was evaluated using four methods. In the steady state, the sliding-mode chattering is reduced under the action of the adaptive term; the observer resists noise disturbances. As shown in Fig. 11, the proposed method exhibits lower current chattering. The maximum speed fluctuations for four methods are 2.3, 1.8, 1.8, and 1.6 r/min, respectively. To analyze their speed error, the specific comparative results of these four control schemes are presented in Table VIII. The results show that the proposed method has an excellent steady-state response under the influence of noise.

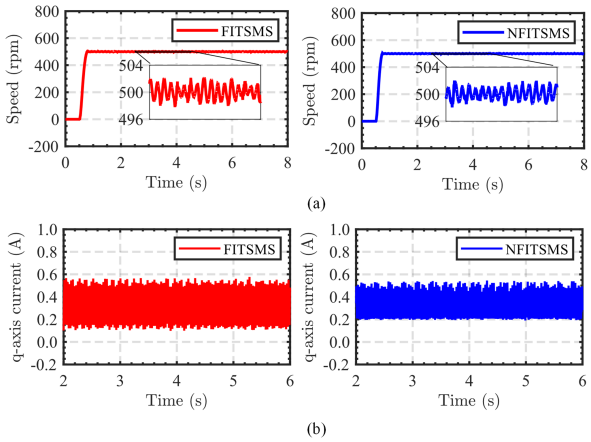

Fig. 12. Speed response and the q-axis current response of different sliding-mode surfaces with 500 r/min. (a) Speed response. (b) q-axis current response.

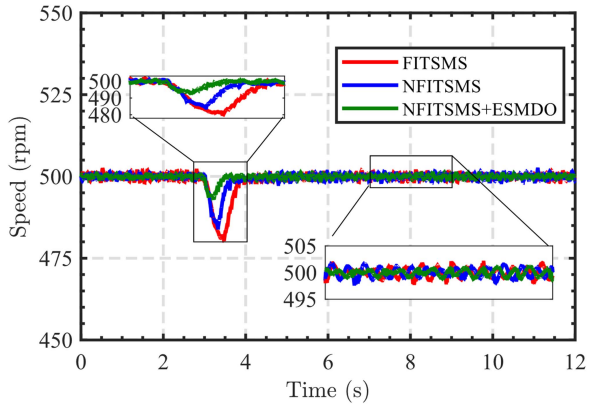

Fig. 13. Speed responses of different sliding-mode surfaces with the load of 1.5 N·m.

E. Speed Response With Different Sliding-Mode Surfaces

To assess the performance of the proposed NFITSMS, the following methods were compared and analyzed: FITSMS [41] with NVGRL, and NFITSMS with NVGRL. As shown in Fig. 12(a), the NFITSMS can make the speed error converge to 0 more quickly; the error can also be further reduced in the steady state. The NFITSMS with the NVGRL achieved a start-up time of 0.328 s, which is significantly faster than the FITSMS, which had a start-up time of 0.393 s. The maximum speed fluctuations for two methods were 2.4 and 1.6 r/min, respectively. The NFITSMS has smaller speed fluctuations and a faster convergence rate, which realizes the global fast convergence in SPMSM speed regulation.

F. Sudden Load Changes With Different Sliding-Mode Surfaces

The reference speed was set to 500 r/min, and speed responses were recorded under a load of 1.5 N·m. When the disturbance is encountered, the sliding-mode function gives the reaching law more power to reach the sliding-mode surface. When the error is small, it still provides a faster convergence rate. As shown in Fig. 13, the settling times for the speed response were 1.202, 1.133, and 0.598 s for the different control methods. The corresponding speed drops for each method were 19, 16, and 8 r/min. At $7 < t < 10$, the speed IAEs were calculated as 0.1715, 0.1529, and 0.1121. The speed RMSEs were calculated as 0.8151, 0.6980, and 0.5658. These indexes show that the proposed new SMC strategy has low speed error, guaranteeing excellent dynamic and steady-state responses for the SPMSM.

V. Conclusion

In this article, a new SMC based on the NVGRL and the NFITSMS combined with the ESMDO was proposed for the SPMSM speed regulation system. The NVGRL was developed to improve the response speed, reduce chattering, and enhance antidisturbance performance. Based on the proposed NVGRL, the NFITSMS was designed to accelerate the error convergence both when the system state is far from and near the equilibrium point, achieving the fast global convergence of the speed error. The ESMDO was introduced to handle uncertainties and external disturbances, and a new sliding-mode controller was designed accordingly. The experimental results demonstrated that the proposed controller offers significantly advantages in terms of fast response speed and robust antidisturbance performance. In future work, the proposed method will be applied to the current loop to reduce the harmonic component of the current, which will further optimize the system performance.

References

[1] R. Thike and P. Pillay, "Mathematical model of an interior PMSM with aligned magnet and reluctance torques," *IEEE Trans. Transp. Electrific.*, vol. 6, no. 2, pp. 647–658, Jun. 2020.

[2] W. Xu, A. K. Junejo, Y. Liu, and M. R. Islam, "Improved continuous fast terminal sliding mode control with extended state observer for speed regulation of PMSM drive system," *IEEE Trans. Veh. Technol.*, vol. 68, no. 11, pp. 10465–10476, Nov. 2019.

[3] S. V. Nair, K. Layek, and K. Hatua, "An unequal split dual three-phase PMSM with extended torque-speed characteristics for automotive application," *IEEE Trans. Power Electron.*, vol. 37, no. 10, pp. 12437–12449, Oct. 2022.

[4] Y. Ma, D. Li, Y. Li, and L. Yang, "A novel discrete compound integral terminal sliding mode control with disturbance compensation for PMSM speed system," *IEEE/ASME Trans. Mechatron.*, vol. 27, no. 1, pp. 549–560, Feb. 2022.

[5] B. Xu, L. Zhang, and W. Ji, "Improved non-singular fast terminal sliding mode control with disturbance observer for PMSM drives," *IEEE Trans. Transp. Electrific.*, vol. 7, no. 4, pp. 2753–2762, Dec. 2021.

[6] L. Chen et al., "Sensorless fixed-time sliding mode control of PMSM based on barrier function adaptive super-twisting observer," *IEEE Trans. Power Electron.*, vol. 39, no. 3, pp. 3037–3051, Mar. 2024.

[7] Y. Yin et al., "Disturbance and uncertainty attenuation for speed regulation of PMSM servo system using adaptive optimal control strategy," *IEEE Trans. Transp. Electrific.*, vol. 9, no. 2, pp. 3410–3420, Jun. 2023.

[8] M. Tian, B. Wang, Y. Yu, Q. Dong, and D. Xu, "Robust adaptive resonant controller for PMSM speed regulation considering uncertain periodic and aperiodic disturbances," *IEEE Trans. Ind. Electron.*, vol. 70, no. 4, pp. 3362–3372, Apr. 2023.

[9] T. Tarczewski and L. M. Grzesiak, "Constrained state feedback speed control of PMSM based on model predictive approach," *IEEE Trans. Ind. Electron.*, vol. 63, no. 6, pp. 3867–3875, Jun. 2016.

[10] S. Li and H. Gu, "Fuzzy adaptive internal model control schemes for PMSM speed-regulation system," *IEEE Trans. Ind. Inform.*, vol. 8, no. 4, pp. 767–779, Nov. 2012.

[11] H. Li, S. Wang, Y. Xie, S. Zheng, and P. Shi, "Virtual reference-based fuzzy noncascade speed control for PMSM systems with unmatched disturbances and current constraints," *IEEE Trans. Fuzzy Syst.*, vol. 31, no. 12, pp. 4249–4261, Dec. 2023.

[12] X. Sun, C. Hu, G. Lei, Z. Yang, Y. Guo, and J. Zhu, "Speed sensorless control of SPMSM drives for EVs with a binary search algorithm-based phase-locked loop," *IEEE Trans. Veh. Technol.*, vol. 69, no. 5, pp. 4968–4978, May 2020.
[13] T. H. Nguyen, T. T. Nguyen, V. Q. Nguyen, K. M. Le, H. N. Tran, and J. W. Jeon, "An adaptive sliding-mode controller with a modified reduced-order proportional integral observer for speed regulation of a permanent magnet synchronous motor," *IEEE Trans. Ind. Electron.*, vol. 69, no. 7, pp. 7181–7191, Jul. 2022.
[14] X. Zhang, L. Sun, K. Zhao, and L. Sun, "Nonlinear speed control for PMSM system using sliding-mode control and disturbance compensation techniques," *IEEE Trans. Power Electron.*, vol. 28, no. 3, pp. 1358–1365, Mar. 2013.
[15] A. K. Junejo, W. Xu, C. Mu, M. M. Ismail, and Y. Liu, "Adaptive speed control of PMSM drive system based a new sliding-mode reaching law," *IEEE Trans. Power Electron.*, vol. 35, no. 11, pp. 12110–12121, Nov. 2020.
[16] K. Han, M. Choi, B. Lee, and S. B. Choi, "Development of a traction control system using a special type of sliding mode controller for hybrid 4WD vehicles," *IEEE Trans. Veh. Technol.*, vol. 67, no. 1, pp. 264–274, Jan. 2018.
[17] X. Sun, J. Cao, G. Lei, Y. Guo, and J. Zhu, "A composite sliding mode control for SPMSM drives based on a new hybrid reaching law with disturbance compensation," *IEEE Trans. Transp. Electrific.*, vol. 7, no. 3, pp. 1427–1436, Sep. 2021.
[18] C. J. Fallaha, M. Saad, H. Y. Kanaan, and K. Al-Haddad, "Sliding-mode robot control with exponential reaching law," *IEEE Trans. Ind. Electron.*, vol. 58, no. 2, pp. 600–610, Feb. 2011.
[19] Z. Zhang, X. Yang, W. Wang, K. Chen, N. C. Cheung, and J. Pan, "Enhanced sliding mode control for PMSM speed drive systems using a novel adaptive sliding mode reaching law based on exponential function," *IEEE Trans. Ind. Electron.*, vol. 71, no. 10, pp. 11978–11988, Oct. 2024.
[20] S. Li, M. Zhou, and X. Yu, "Design and implementation of terminal sliding mode control method for PMSM speed regulation system," *IEEE Trans. Ind. Informat.*, vol. 9, no. 4, pp. 1879–1891, Nov. 2013.
[21] P. Mani, R. Rajan, L. Shanmugam, and Y. H. Joo, "Adaptive fractional fuzzy integral sliding mode control for PMSM model," *IEEE Trans. Fuzzy Syst.*, vol. 27, no. 8, pp. 1674–1686, Aug. 2019.
[22] H. Komurcugil, S. Bayhan, N. Guler, and H. Abu-Rub, "A new exponential reaching law approach to the sliding mode control: A multilevel multifunction converter application," *IEEE Trans. Ind. Electron.*, vol. 70, no. 8, pp. 7557–7568, Aug. 2023.
[23] W. B. Gao and J. C. Hung, "Variable structure control of nonlinear systems: A new approach," *IEEE Trans. Ind. Electron.*, vol. 40, no. 1, pp. 45–55, Feb. 1993.
[24] H. Ma, Y. Li, and Z. Xiong, "Discrete-time sliding-mode control with enhanced power reaching law," *IEEE Trans. Ind. Electron.*, vol. 66, no. 6, pp. 4629–4638, Jun. 2019.
[25] L. Chen, H. Zhang, H. Wang, K. Shao, G. Wang, and A. Yazdani, "Continuous adaptive fast terminal sliding mode-based speed regulation control of PMSM drive via improved super-twisting observer," *IEEE Trans. Ind. Electron.*, vol. 71, no. 5, pp. 5105–5115, May 2024.
[26] H. Wang et al., "Continuous fast nonsingular terminal sliding mode control of automotive electronic throttle systems using finite-time exact observer," *IEEE Trans. Ind. Electron.*, vol. 65, no. 9, pp. 7160–7172, Sep. 2018.
[27] Y. Wang, Y. Zhu, X. Zhang, B. Tian, K. Wang, and J. Liang, "Antidisturbance sliding mode-based deadbeat direct torque control for PMSM speed regulation system," *IEEE Trans. Transp. Electrific.*, vol. 7, no. 4, pp. 2705–2714, Dec. 2021.
[28] F. Wang, L. He, and J. Roseguez, "A robust predictive speed control for SPMSM systems using a sliding mode gradient descent disturbance observer," *IEEE Trans. Energy Convers.*, vol. 38, no. 1, pp. 540–549, Mar. 2023.
[29] B. Cavus and M. Akdas, "A new adaptive terminal sliding mode speed control in flux weakening region for DTC controlled induction motor drive," *IEEE Trans. Power Electron.*, vol. 39, no. 1, pp. 449–458, Jan. 2024.
[30] E. Kim, "A fuzzy disturbance observer and its application to control," *IEEE Trans. Fuzzy Syst.*, vol. 10, no. 1, pp. 77–84, Feb. 2002.
[31] I. C. Baik, K. H. Kim, and M. J. Youn, "Robust nonlinear speed control of PM synchronous motor using boundary layer integral sliding mode control technique," *IEEE Trans. Control Syst. Technol.*, vol. 8, no. 1, pp. 47–54, Jan. 2000.
[32] X. Yu, Y. Feng, and Z. Man, "Terminal sliding mode control—An overview," *IEEE Open J. Ind. Electron. Soc.*, vol. 2, pp. 36–52, 2021.
[33] Z. Li, F. Wang, D. Ke, J. Li, and W. Zhang, "Robust continuous model predictive speed and current control for PMSM with adaptive integral sliding-mode approach," *IEEE Trans. Power Electron.*, vol. 36, no. 12, pp. 14398–14408, Dec. 2021.
[34] L. Zhang, L. Liu, Z. Wang, and Y. Xia, "Continuous finite-time control for uncertain robot manipulators with integral sliding mode," *IET Control Theory Appl.*, vol. 12, no. 11, pp. 1621–1627, Jul. 2018.
[35] W. Xu, A. K. Junejo, Y. Liu, M. G. Hussien, and J. Zhu, "An efficient antidisturbance sliding-mode speed control method for PMSM drive systems," *IEEE Trans. Power Electron.*, vol. 36, no. 6, pp. 6879–6891, Jun. 2021.
[36] X. Zhang and Z. Li, "Sliding-mode observer-based mechanical parameter estimation for permanent magnet synchronous motor," *IEEE Trans. Power Electron.*, vol. 31, no. 8, pp. 5732–5745, Aug. 2016.
[37] J. Davila, L. Fridman, and A. Poznyak, "Observation and identification of mechanical systems via second order sliding modes," *Int. J. Control*, vol. 79, no. 10, pp. 1251–1262, Oct. 2006.
[38] Z. Yang, J. Sun, X. Sun, B. Wang, and L. Feng, "Direct instantaneous torque control for six-phase SRM with nonsingular fast terminal sliding mode controller," *IEEE J. Emerg. Sel. Top. Power Electron.*, vol. 12, no. 1, pp. 505–515, Feb. 2024.
[39] S. P. Bhat and D. S. Bernstein, "Finite-time stability of continuous autonomous systems," *SIAM J. Control Optim.*, vol. 38, no. 3, pp. 751–766, Jan. 2000.
[40] Z. Zhang and X. Liu, "An improved super-twisting sliding mode single-loop control with current-constraint for PMSM based on two-time scale disturbance observer," *IEEE Trans. Transp. Electrific.*, vol. 10, no. 3, pp. 5389–5399, Sep. 2024.
[41] F. Wang and L. He, "FPGA-based predictive speed control for PMSM system using integral sliding-mode disturbance observer," *IEEE Trans. Ind. Electron.*, vol. 68, no. 2, pp. 972–981, Feb. 2021.

Cao Li was born in Anhui, China, in 1997. He is currently working toward the Ph.D. degree in electrical engineering with the School of Electrical Engineering and Automation, Anhui University, Hefei, China.

His research interests include sliding-mode control and its application to permanent magnet synchronous motors.

Tianhong Pan (Senior Member, IEEE) received the Ph.D. degree in control theory and control engineering from Shanghai Jiaotong University, Shanghai, China, in 2007.

He is currently a Professor with the School of Electrical Engineering and Automation, Anhui University, Hefei, China. His research interests include multiple-model approach and its application, machine learning, virtual metrology, predictive control, and run-to-run control theory and practice.

Shihong Ding (Senior Member, IEEE) received the B.E. degree in mathematics from Anhui Normal University, Wuhu, China, in 2004, and the M.S. and Ph.D. degrees in automatic control from Southeast University, Nanjing, China, in 2007 and 2010, respectively.

From 2008 to 2009, during the graduate studies, he visited the University of Texas at San Antonio, San Antonio, TX, USA. After graduation, he held a Research Fellowship with the University of Western Sydney, Penrith, NSW, Australia, for one year. From July to August 2018, he visited Yeungnam University, Gyeongsan, South Korea. From December 2019 to February 2020, he was also visited RMIT University, Melbourne, VIC, Australia. Since June 2010, he has been with the School of Electrical and Information Engineering, Jiangsu University, Zhenjiang, China, where he is currently a Full Professor. His research interests include sliding-mode control and finite-time stability.